

LUMINOSITY FUNCTIONS OF THE GALAXY CLUSTER MS 1054–0321
AT $z = 0.83$ BASED ON ACS PHOTOMETRY

TOMOTSUGU GOTO,¹ MARC POSTMAN,² NICHOLAS J. G. CROSS,¹ G. D. ILLINGWORTH,³ K. TRAN,⁴ D. MAGEE,³
M. FRANX,⁵ N. BENÍTEZ,¹ R. J. BOUWENS,³ R. DEMARCO,¹ H. C. FORD,¹ N. L. HOMEIER,¹ A. R. MARTEL,¹
F. MENANTEAU,¹ M. CLAMPIN,⁶ G. F. HARTIG,² D. R. ARDILA,¹ F. BARTKO,⁷ J. P. BLAKESLEE,¹
L. D. BRADLEY,¹ T. J. BROADHURST,⁸ R. A. BROWN,² C. J. BURROWS,² E. S. CHENG,⁹
P. D. FELDMAN,¹ D. A. GOLIMOWSKI,¹ C. GRONWALL,¹⁰ B. HOLDEN,³ L. INFANTE,¹¹
M. J. JEE,¹ J. E. KRIST,² M. P. LESSER,¹² S. MEI,¹ G. R. MEURER,¹ G. K. MILEY,⁵
V. MOTTA,^{1,11} R. OVERZIER,^{1,5} M. SIRIANNI,^{2,13} W. B. SPARKS,² H. D. TRAN,¹⁴

The cluster galaxy luminosity function (LF) is a fundamental constraint on the mass assembly history of galaxy clusters as it is related to the cluster galaxy mass function through the mass-to-light ratio. Precise and accurate measurements of cluster LFs as a functions of local galaxy density, clustocentric radius, galaxy structure, and color have the potential to provide insight into the role of environmental processes in determining the properties of the present-day galaxy populations. The LF is therefore central to many cosmological issues (Koo & Kron 1992; Ostriker 1993; Binggeli & Jerjen 1998; Binggeli et al. 1988).

In the local universe, the cluster galaxy LFs have been studied in considerable detail at optical and near-infrared wavelengths (e.g., Lugger 1986; Trentham 1998; Garilli et al. 1999; Paolillo et al. 2001; Martínez et al. 2002; Cuesta-Bolao & Serna 2003; De Propris et al. 2003; Lin et al. 2004). Goto et al. (2002b) derived the composite luminosity function of 204 clusters from the SDSS Cut and Enhance Galaxy Cluster Catalog (Goto et al. 2002a) in the redshift range from $z = 0.02$ to 0.25 in the five SDSS bands u^* , g^* , r^* , i^* , and z^* , and found that the faint-end slope of the luminosity function becomes flatter toward the redder wavebands, consistent with the hypothesis that the cluster luminosity function has two distinct underlying populations; a population of bright elliptical galaxies with a Gaussian-like luminosity distribution that dominate the bright end, and a population of faint blue star-forming galaxies with a steep power-law-like luminosity distribution, that dominate the faint-end. Indeed, several studies find that cluster LFs are better described by a sum of two functions; a Gaussian for bright galaxies and a steep Schechter function for faint galaxies (Driver et al. 1994; Molinari et al. 1998; Parolin et al. 2003; Mercurio et al. 2003; Dahlén et al. 2004), consistent with the above picture. De Propris et al. (1998) derived the H -band luminosity function of the Coma cluster galaxies, providing further support to the hypothesis of distinct populations: intrinsically bright red galaxies and intrinsically faint blue dwarf galaxies. The dwarf-to-giant ratio also appears to depend on environment. Several studies (Driver et al. 1998; Phillipps et al. 1998; Andreon 2001; Dahlén et al. 2004) find that dwarf galaxies are more common in lower density environments in local clusters.

It is important to extend these studies to higher redshifts, as the evolution of the above characteristics can provide useful discrimination among structure formation and evolution models. To date, however, only a handful of clusters at $z \sim 1$ have been studied in detail (Stanford et al. 1997; Benítez et al. 1999; Rosati et al. 1999; Tanaka et al. 2000; Haines et al. 2001; van Dokkum et al. 2001; Lidman et al. 2004). In addition, most of these studies relied on photometric redshifts to determine cluster membership. The evolution of the K -band luminosity function in the redshift range $z = 0.1$ – 0.9 has been studied by De Propris et al. (1999). The evolution of the characteristic magnitude K^* of the galaxies is found to be consistent with a passively evolving population of galaxies formed at $z_f > 2$. The data are not deep enough, however, to constrain the faint-end slope, which was fixed at $\alpha = -0.9$ in the above study (and adopted from the value derived in the H band for the Coma Cluster). Nakata et al. (2001) extended the study to $z = 1.2$ by deriving the K -band luminosity function for the cluster around the radio galaxy 3C 324. They also chose to fix the faint-end slope at $\alpha = -0.9$ and found a result consistent with what is expected for a passively evolving stellar population formed at $z_f > 2$. Toft et al. (2004) studied the K -band LF of galaxy cluster RDCS J1252.9–2927 at $z = 1.237$. They found $\Delta M_z^* = 1.3 \pm 0.5$ mag of evolution and a similar shape for the faint-end tail. The main difficulties in studying cluster galaxy populations

at $z \sim 1$ are, of course, the fainter apparent magnitude of the distant cluster galaxies and contamination by non-cluster member galaxies.

With the advent of the Advanced Camera Surveys (ACS) on board the *Hubble Space Telescope* (*HST*), we now have a chance to step forward. As a part of Guaranteed Time Observations (GTO), we have observed the galaxy cluster MS 1054–0321 at $z = 0.83$. A large companion spectroscopic campaign yielded redshifts for 143 cluster members, eliminating the uncertainties associated with photometric redshift estimation or statistical background subtraction (Driver et al. 1994; Bernstein et al. 1995; Valotto et al. 2001). The superb sensitivity and angular resolution of the ACS allows us to classify galaxies morphologically to the depth of $i_{775} = 24$ mag.

We present in this paper our ACS-based LF and its dependence on clustocentric position, environment, and galaxy properties for the galaxy cluster MS 1054–0321 at $z = 0.83$. The paper is organized as follows. In § 2, we describe the observations; in § 3, we describe the details of the analysis; in § 4, we present the results; in § 5, we discuss the physical implications of our results; and in § 6, we summarize our work and findings. Unless otherwise stated, we adopt the best-fit *WMAP* cosmology, $h = 0.71$, $\Omega_m = 0.27$, $\Omega_L = 0.73$ (Bennett et al. 2003), giving a scale of 7.62 kpc arcsec $^{-1}$ at $z = 0.83$.

2. DATA

2.1. MS 1054–0321

With a redshift of $z = 0.831$, MS 1054–0321 is the most distant cluster in the Extended Medium Sensitivity Survey (EMSS) X-ray-selected cluster sample (Gioia et al. 1990). It has a rest-frame X-ray luminosity of $L_X(2\text{--}10 \text{ keV}) = 2.2 \times 10^{45} h_{50}^{-1} \text{ ergs s}^{-1}$ (Donahue et al. 1998), which makes it one of the brightest X-ray clusters known. With *Chandra* ACIS-S, Jeltema et al. (2001) found the X-ray temperature of the cluster to be $10.4_{-1.5}^{+1.7}$ keV, with an iron abundance of 0.26 ± 0.15 relative to solar. However, more recent observations with *XMM* (Gioia et al. 2004) indicate the temperature could be as low as $7.2_{-0.6}^{+0.7}$ keV. The difference in temperature is in part related to differences among authors in the procedures used in its derivation. A fair compromise is $T_X = 8.0_{-1.5}^{+2.5}$ keV (M. Donahue 2004, private communication). MS 1054–0321 has an Abell richness class of 3 and a line-of-sight velocity dispersion of $\sigma = 1170 \pm 150 \text{ km s}^{-1}$ (Tran et al. 1999). The weak-lensing mass is estimated to be $9.89 \pm 0.36 \times 10^{14} M_\odot$ (Jee et al. 2005).

A significant fraction of cluster galaxies, 17%, are classified as “merger/peculiar” on the basis of double nuclei (separation < 10 kpc), tidal tails, and distorted morphologies (van Dokkum et al. 1999). Interestingly, many of the merging galaxies are red, bulge-dominated galaxies with no detected nebular line emission. The fraction of blue galaxies in the cluster, calculated in the same way as the original work by Butcher & Oemler (1978, 1984), is 0.22 ± 0.05 (van Dokkum et al. 2000), comparable with the mean value determined for clusters at $0.3 < z < 0.5$ (e.g., Goto et al. 2003b, 2004a).

2.2. HST ACS and Keck LRIS Observations

We have observed MS 1054–0321 in the F606W, F775W, and F850LP bandpasses (hereafter V_{606} , i_{775} , and z_{850} , respectively) with the Wide Field Channel (WFC) of ACS as a part of the GTO program 9290. A mosaic observation was constructed using a 2×2 WFC pointing pattern, with 1, 2, and 2 orbits of integration in V_{606} , i_{775} , and z_{850} bands, respectively, at each of the four pointings. There was nearly $1'$ of overlap between

pointings; thus, the core of cluster was imaged for a total of 8 orbits in i_{775} and z_{850} . The field of view of the mosaic is 36.51 square arcminutes, covering an approximately square geometry with a projected proper spatial dimension of 2.7 Mpc at $z = 0.83$. The data were processed with the “Apsis” pipeline described by Blakeslee et al. (2003). We use the SExtractor MAG_AUTO value output by the pipeline for our photometric measure. This magnitude is intended to give a precise estimate of total magnitudes for galaxies using Kron’s first-moment algorithm (Blakeslee et al. 2003). We calibrate our photometry to the AB system using photometric zero points of 26.48 (V_{606}), 25.65 (i_{775}), and 24.86 (z_{850}). These are uncertain at the ~ 0.02 mag level, which has no effect on our conclusions. We adopt a Galactic reddening for this field of $A_V = 0.0945$, $A_i = 0.0714$, and $A_z = 0.0521$ mag based on the Schlegel et al. (1998) dust maps.

Multiobject spectroscopy of the galaxies in region was carried out on the Keck Telescope using the Low Resolution Imaging Spectrograph (Oke et al. 1995). This survey has yielded redshifts for over 300 objects, with 143 of these being confirmed as cluster members (van Dokkum et al. 2000; K. H. Tran et al. 2005, in preparation). Spectroscopic redshifts are measured for 76% of the galaxies brighter than $i_{775} = 22.0$ (see § 3.2). The availability of this extensive spectroscopic database provides a significant advantage in studying the galaxy cluster MS 1054–0321. To obtain a large number of spectroscopic memberships in galaxy clusters at $z \sim 1$, a large amount of telescope time is usually required, and thus most previous studies had to rely on the photometric redshift estimation or the statistical background subtraction, both of which were the main source of bias in determining the slope of the LF at the faint end (Driver et al. 1994; Bernstein et al. 1995; Valotto et al. 2001). We exclusively use the spectroscopically confirmed cluster members to construct the LF in MS 1054–0321.

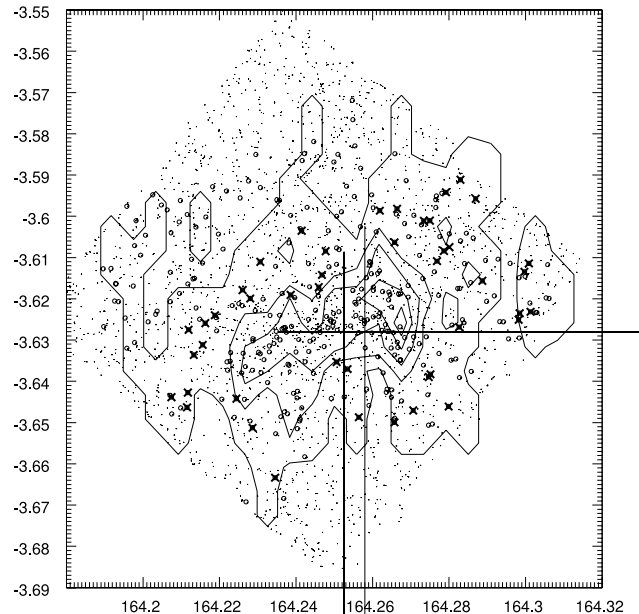
3. ANALYSIS

3.1. Cluster Membership Determination

We regard the 143 galaxies with $0.81 < z < 0.85$ as members of MS 1054–0321. This corresponds to a rest-frame spread of ± 3300 km s $^{-1}$ about the mean cluster redshift. After correcting to the cluster rest frame and subtracting the contribution to the observed velocity dispersion from the redshift measurement errors (~ 200 km s $^{-1}$), we find a line-of-sight cluster velocity dispersion of 1131 ± 5 km s $^{-1}$ (measured as a σ of biweighted mean with the jackknife error estimate). The derived line-of-sight velocity dispersion is consistent with previously published numbers (e.g., Tran et al. 1999; Goto et al. 2004b).

3.2. Correction for Incompleteness in Spectroscopic Sample

Incompleteness in measuring spectroscopic redshifts (or targeting galaxies for observation) as a function of apparent magnitude must be compensated for in order to extract unbiased results. Figure 1 shows the sky distribution of objects with spectroscopy (*open circles*) and all extended objects in the imaging data (*small dots*). Since we have only performed spectroscopic observations in the region defined by the solid lines, we use objects within this region to define and quantify the incompleteness (for more details of the spectroscopic observations, see van Dokkum et al. 1999, 2000; Postman et al. 2005; K. H. Tran et al. 2005, in preparation). Point sources are excluded from incompleteness calculations using SExtractor’s stellarity index ($\text{CLASS_STAR} > 0.5$), which assigns a numerical value close to 1 if the object is a point source and values closer to 0



if it is an extended object. A slight change in the criterion of the separation between extended and point sources (e.g., using a CLASS_STAR value of 0.8 instead of 0.5 as the threshold) does not affect our results. In Figure 2, we show the fraction of galaxies that have a spectroscopic redshift among all galaxies in the imaging data as a function of apparent i_{775} magnitude. As can be seen in Figure 2, the completeness is almost independent of magnitude in the range of $18.0 < i_{775} < 22.0$, indicating that the spectroscopic survey is not strongly biased and has a high degree of completeness. Regardless, when we measure a LF in the following sections, we correct for the incompleteness by weighting the observed counts by the inverse of the completeness.

In the following analyses, we divide our cluster galaxy sample using various criteria in morphology, environment, and color. When measuring LFs of these subsamples, the incompleteness correction is recomputed using each subsample of galaxies, and then applied to the LFs of each subsample accordingly. As an example, we plot the spectroscopic completeness for blue ($i_{775} - z_{850} < 0.5$) and red ($i_{775} - z_{850} \geq 0.5$) subsamples with dashed and dotted lines in Figure 2. It can be seen that the completeness is not strongly dependent on $i_{775} - z_{850}$ color. When we construct a LF in different passbands (V_{606} , i_{775} , and z_{850}), we correct the counts using the incompleteness as a function of magnitude in that passband.

3.3. Quantifying the Environment of Galaxies

Because different physical mechanisms that act on galaxies in dense environments have efficiencies that vary as a function of density or position, we quantify the LF as a function of these variables in hopes of understanding the underlying processes (see a review in Treu et al. 2003).

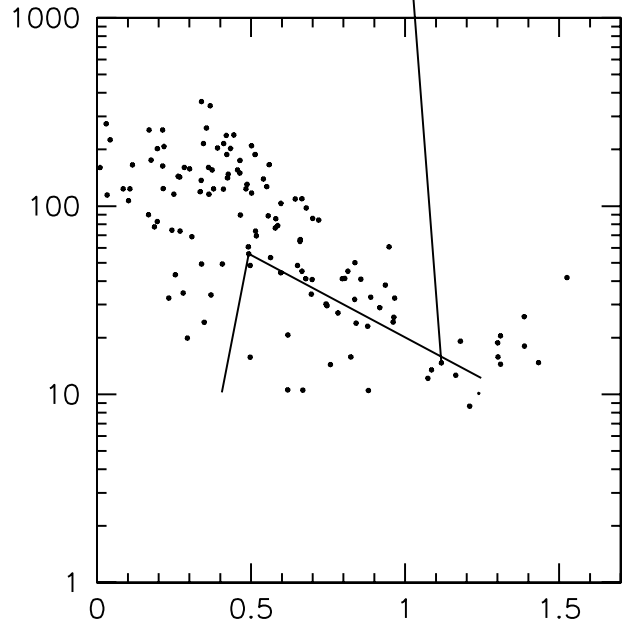
3.3.1. Local Galaxy Density

For each galaxy, we measure a projected (angular) distance to the 5th nearest galaxy using the cluster members ($0.81 < z < 0.85$)

The number of galaxies ($N = 5$) within the distance is divided by the circular surface area with the radius of the distance to the 5th nearest galaxy to obtain the local galaxy density, Σ (Mpc^{-2}). When the projected area touches the boundary of the data (Fig. 1), we calculate the density by dividing the area within the data region. This parameterization is similar to the one used in previous work (e.g., Goto et al. 2003a, 2003c; Tanaka et al. 2004). Although our local galaxy density is a two-dimensional surface density, the contamination from both foreground and background galaxies is zero, because we are using spectroscopic information. However, because we do not have spectroscopic redshifts for all the members, our measured density is an underestimate. We use this density only for internal comparisons. We have chosen the 5th nearest to measure local galaxy density, but we also have confirmed that using up to the 10th nearest neighbor does not change the main results described below.

3.3.2. Clustocentric Distance

To assess dependencies of the LF on position within the cluster, we measure the projected distance to the cluster center, R , for all spectroscopically confirmed member galaxies. We use the position of the brightest cluster galaxy (R.A. = $10^{\text{h}}56^{\text{m}}59^{\text{s}}.99$, decl. = $-03^{\circ}37'36''.1$ [J2000.0]) as the center of the cluster. Using the centroid of the X-ray surface brightness distribution (Neumann & Arnaud 2000) does not significantly change the results. The virial radius of the cluster is known to be ~ 1 Mpc (Tran et al. 1999). In Figure 3, we compare the clustocentric distance with the local galaxy density. The solid lines connect medians. The error bars are based on the rms in each bin. As expected, there is a fairly good correlation between these two parameters. Note that the clustocentric distance of $R = 0.9$ Mpc corresponds to $30\text{--}40 \text{ Mpc}^{-2}$ in local galaxy density.



3.4. Luminosity Function Measurements

We use a nonlinear least-squares method to determine the best-fit Schechter (1976) LF parameters. The LF normalization (ϕ^*), faint-end slope (α), and characteristic magnitude (M^*) are fit simultaneously. The input data for the fitting procedure is a binned, apparent magnitude distribution for the spectroscopically confirmed cluster members, where the number of galaxies in each bin has been corrected for incompleteness in the spectroscopic survey. We use a magnitude bin size of 0.5 mag. The values of the best-fit LF parameters do not strongly depend on our choice of the bin size in the range $0.25 < \delta m < 0.75$. The incompleteness correction is determined empirically by dividing the number of objects with measured redshifts in a given apparent magnitude bin by the total number of galaxies in that same bin. The total number of galaxies in a bin is taken from our SExtractor catalog. The corrected number counts as a function of apparent magnitude are then converted to the corresponding absolute magnitude using a distance modulus of $m - M = 42.86$. We do not apply K -corrections for the internal MS 1054 LF comparisons. However, whenever we compare our results to those from other studies, a K -correction is applied and the details of how the K -correction is determined are given in § 5.1. Finally, we divide the corrected number counts by the effective area of the survey (in units of projected Mpc^2 ; see Fig. 1). All fits are weighted by the inverse square of the error in the galaxy number in each bin, and these errors are determined from Poisson statistics using the original (uncorrected) number counts. The best-fit Schechter parameters for all samples are summarized in Table 1.

4. RESULTS

4.1. Luminosity Function of Galaxy Cluster MS 1054–0321

With the spectroscopic membership information and parameters to describe the environment of each galaxy in hand, it is straightforward to construct a LF of the member galaxies. It is desirable to normalize the absolute magnitude to $h = 1$ for external comparison purposes, and we thus adopt the distance

m
F
in
us
P
ob
su
sh
S
of
a
m
fi
(M
(-
m
de
G
te

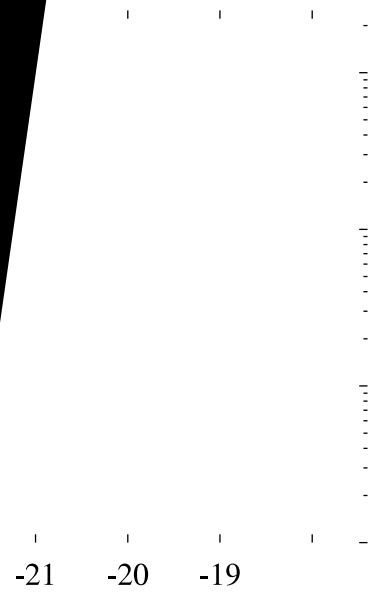
which is clearly seen
corresponds to the rest-
LF in V_{606} and the
between star-forming
LFs with those in the

Function ce

of the LF on environ-
galaxy luminosity dis-
distance. In the upper
the inner ($R < 0.9$ Mpc)
054–0321. The thresh-
to the distance at which
significant changes inward to-
with $R < 0.9$ Mpc has a
a flatter faint-end slope
we fit a Schechter function
results in the lower panel of
each data point. These error
best-fit Schechter parameters
 -28 ± 0.35 and $-20.77 \pm$
with $R \geq 0.9$ and $R < 0.9$,
deeper faint-end slope is de-
 $R \geq 0.9$ Mpc) as compared
in the inner cluster region.
with the findings in the
the literature (e.g., Goto et al.
different environments suggests
a role in determining the lu-

tion as a Function axy Density

6, we plot the LF of the cluster
density of 30 Mpc^{-2} . The solid



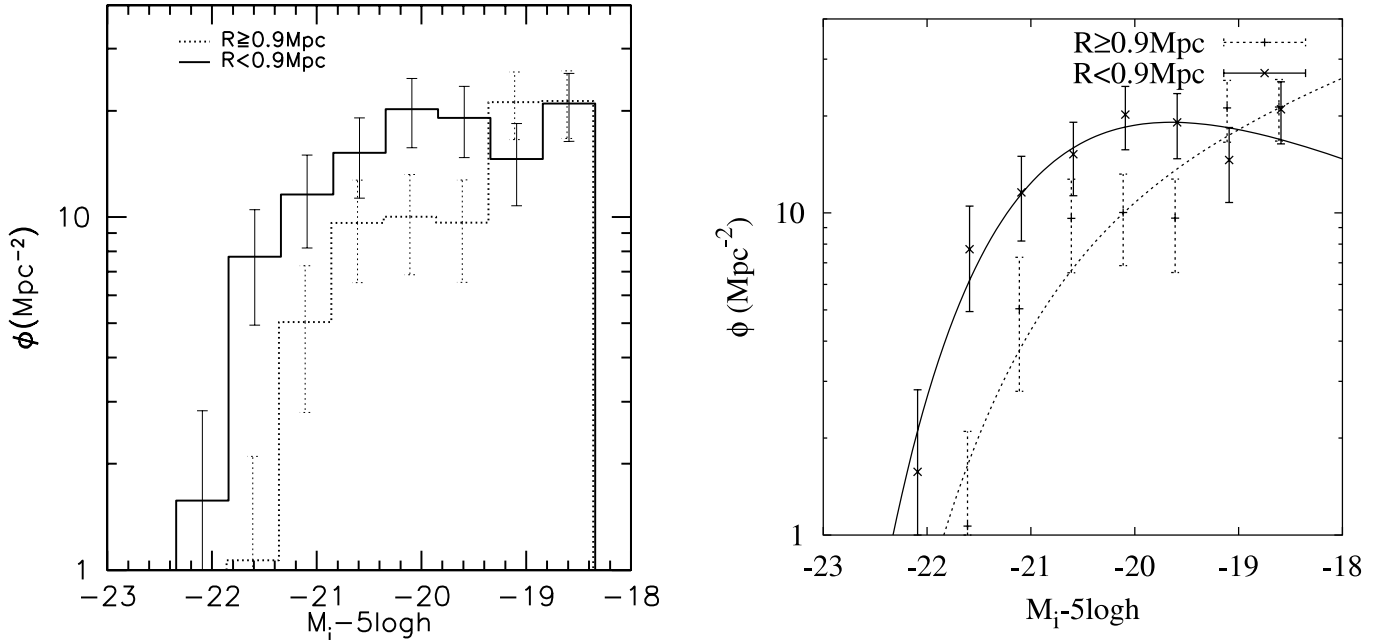


FIG. 5.—Luminosity function with spectroscopic members partitioned by the distance from the cluster center. The solid line uses galaxies within 0.9 Mpc from the cluster center determined by the position of the brightest cluster galaxy. The dotted line uses galaxies outside of 0.9 Mpc from the cluster center.

line is for galaxies in regions with $\Sigma \geq 30 \text{ Mpc}^{-2}$, and the dashed line is for galaxies in regions with $\Sigma < 30 \text{ Mpc}^{-2}$. Again, the criterion of $\Sigma = 30 \text{ Mpc}^{-2}$ is chosen to correspond to the environment where galaxy properties start to exhibit substantial change relative to the field galaxy population (see § 4.6). The LF of galaxies in dense regions has a flatter faint-end slope than in sparse environments, consistent with the results obtained as a function of clustocentric radius. Note that we do not normalize the LFs in Figure 6 because the sampling volume of each galaxy is different as a consequence of the way the local galaxy density is measured (§ 3.3.1).

In the lower panel, we fit a Schechter function to each LF. The best-fit Schechter parameters are $(M_i^*, \alpha) = (-21.43 \pm 0.71,$

$-1.42 \pm 0.25)$ and $(-20.63 \pm 0.15, -0.53 \pm 0.12)$ for galaxies with $\Sigma < 30 \text{ Mpc}^{-2}$ and $\Sigma \geq 30 \text{ Mpc}^{-2}$, respectively. These results are also given in Table 1. Although the errors on the parameters are substantial, the parameter values are consistent with the interpretation that the galaxy LF in dense regions has a flatter faint-end slope.

4.4. Luminosity Function as a Function of Color

The i_{775} filter is particularly sensitive to different stellar populations at $z = 0.83$ because it includes the 4000 \AA break. In particular, the $i_{775} - z_{850}$ color does a reasonable job of distinguishing blue, star-forming galaxies from red, passive galaxies in the color-magnitude relation (N. L. Homeier et al. 2005, in

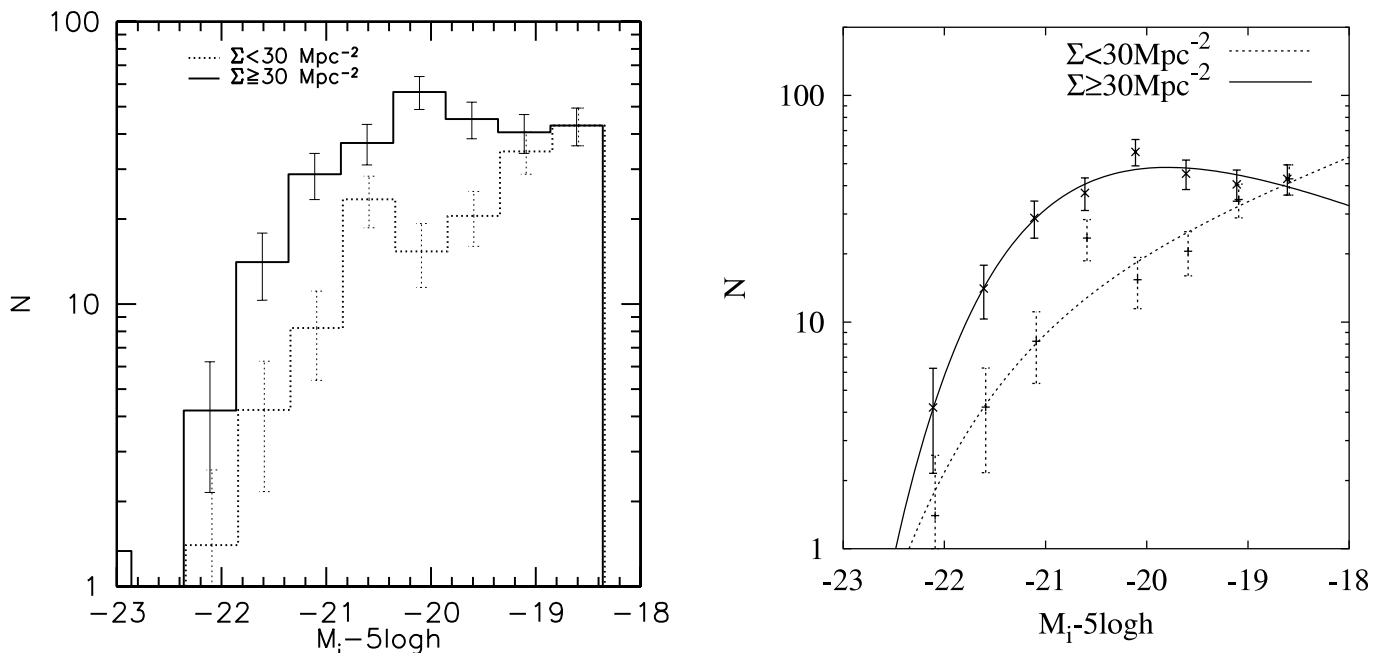


FIG. 6.—Luminosity function partitioned by the local galaxy density. The solid and dashed lines use galaxies with the local galaxy density greater than and less than 30 Mpc^{-2} , respectively. Since both the high-density and low-density samples are specially spread over the entire sky area, the same (overall) incompleteness corrections are applied to the both LFs.

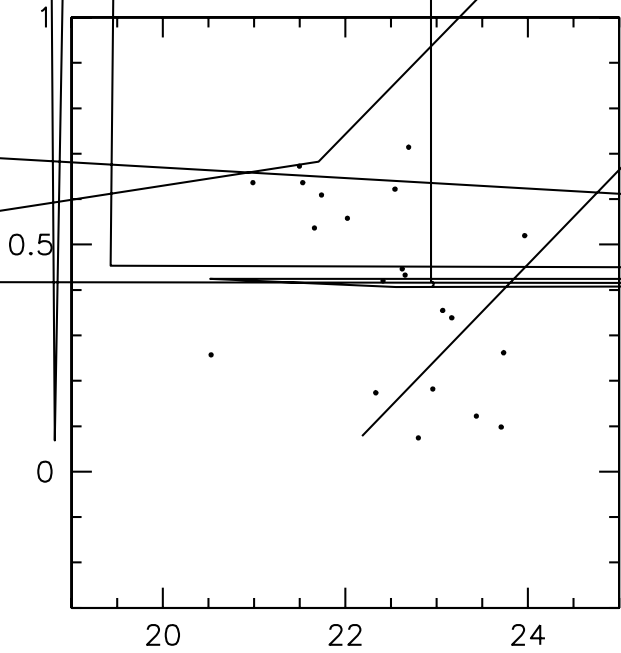


Figure 8 with best-fit parameters of $(M_i^*, \alpha) = (-20.11 \pm 0.22, -0.09 \pm 0.27)$, $(-21.92 \pm 0.86, -1.48 \pm 0.23)$ for red and blue samples, respectively. One potentially interesting difference is that the LF of red galaxies shows a deficit at the faint end $M_i^* > -19$. Similar deficits of faint red galaxies in high-redshift galaxy samples have been reported in the literature (e.g., Kajisawa et al. 2000; Nakata et al. 2001; Kodama et al. 2004; De Lucia et al. 2004). Such a deficit may signal the presence of galaxy population that has yet to evolve into a faint, red phase. We discuss this hypothesis and its implication further in § 5.

4.5. Luminosity Function as a Function of Galaxy Morphology

In addition to providing superb quality photometry, a key advantage provided by the high angular resolution provided by *HST* and the ACS, in particular, is the ability to classify galaxy morphology out to redshifts as high as $z = 0.83$. One of us (M. P.) has visually classified the morphology of MS 1054–0321 galaxies with $i_{775} < 24$ (see Postman et al. 2005 for further details). We use these classifications here to examine how the luminosity distribution depends on morphology. In Figure 9, we present a LF of early-type galaxies (E+S0 or $T \leq 0$) and that of late-type galaxies (Sa or later; $T > 0$). Our best-fit Schechter parameters are $(M_i^*, \alpha) = (-20.76 \pm 0.12, -0.54 \pm 0.13)$, $(-20.70 \pm 0.12, -0.54 \pm 0.13)$ for early- and late-type

preparation). Figure 7 shows the color-magnitude diagram (CMD) of the known cluster members (*larger filled circles*) and the extended objects in the field (*small dots*). The color-magnitude diagram separates well the galaxies in the red sequence from the blue sequence galaxies. A detailed analysis of the color-magnitude relation in MS 1054–0321 will be presented in Postman et al. (2005, in preparation). The LFs of galaxies with $i_{775} < 24$ are shown by the dashed and solid lines, respectively. The best-fit Schechter functions

are shown in Figure 9. The dashed and solid lines highlight some subtle differences between the LFs of morphologically classified galaxies in Figure 10 with slightly higher early-type fractions. This suggests that the cluster galaxies have a somewhat higher than field galaxies (e.g., Postman et al. 2000). This is due to the star formation process as we expect that galaxies involved in mergers, which are also associated with work at lower redshifts, will have more details in morphology.

Corrections for the incompleteness of spectroscopic observation is corrected for each subsample of galaxies.

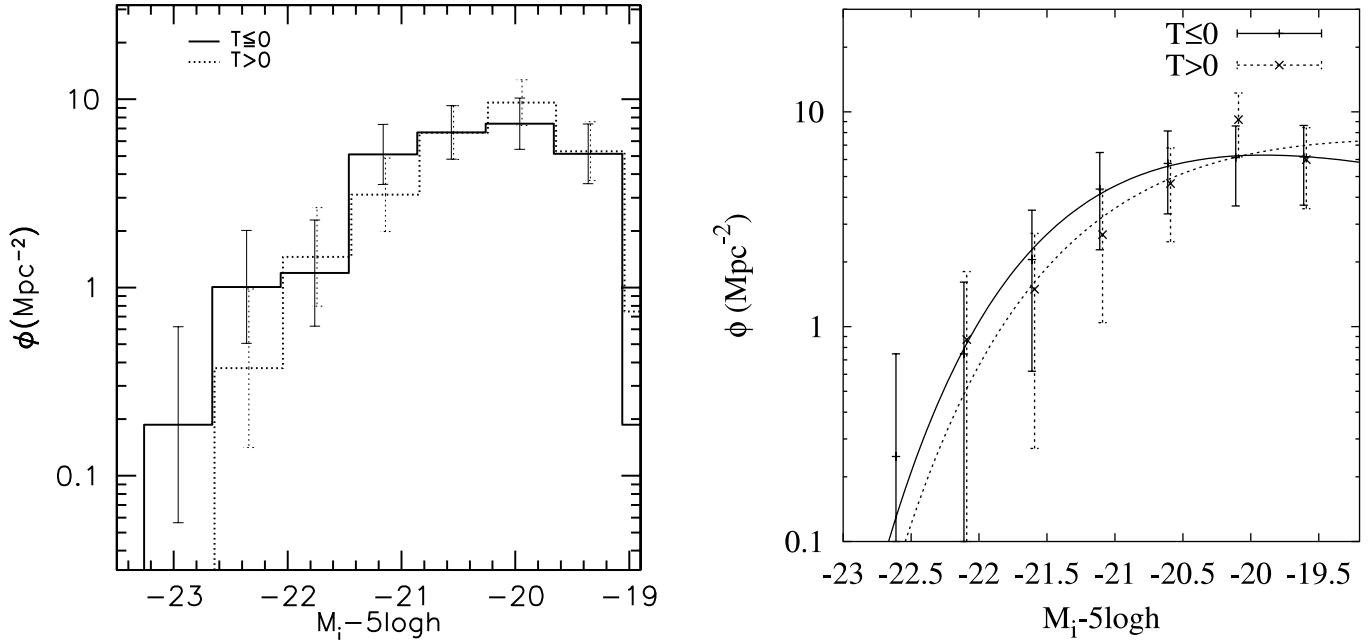


FIG. 9.—LFs divided by morphological type: $T \leq 0$ are E/S0, $T > 0$ are late type. Corrections for incompleteness are applied separately for each morphological sample.

4.6. Giant-to-Dwarf Ratio

In this section, we investigate the giant-to-dwarf ratio (GDR) as functions of color, morphology, clustocentric radius, and local projected density. We calculate the GDR as a number ratio of giant galaxies ($M_i < -19.5$) to dwarf galaxies ($-19.5 \leq M_i < -18.0$) using the expression

$$\text{GDR} = \frac{N(M_i < -19.5)}{N(-19.5 \leq M_i < -18.0)}. \quad (1)$$

The demarcation between dwarf and giant at $M_i = -19.5$ is chosen to correspond approximately to the start of the deviation

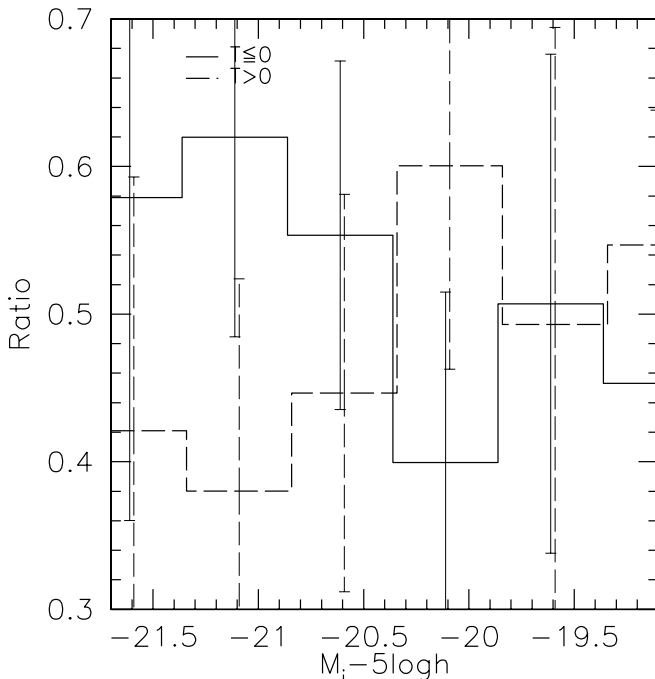


FIG. 10.—Number ratio of early-type ($T \leq 0$; solid line) and late-type ($T > 0$; dashed line) galaxies as a function of absolute magnitude.

between the faint ends of the color-selected LFs in Figure 8. Because of the large distance to the cluster, we cannot sample the dwarf population to as faint magnitudes as were probed in previous studies (~ -16.5 mag; e.g., Ferguson & Sandage 1991; Secker & Harris 1996). Therefore, we take the inverse of the commonly used dwarf-to-giant ratio in order to magnify the subtle change in the parameter. In Figure 11, we show the GDR as a function of $i_{775} - z_{850}$ color. The trend seen in Figure 8 is much clearer here, in the sense that the GDR is much higher for red galaxies, and gradually declines as the galaxy color becomes bluer. In Figure 12, we show the GDR as a function of morphological type. Confirming the trend seen in Figure 9, the GDR is higher for early-type ($T \leq 0$) galaxies. These two trends

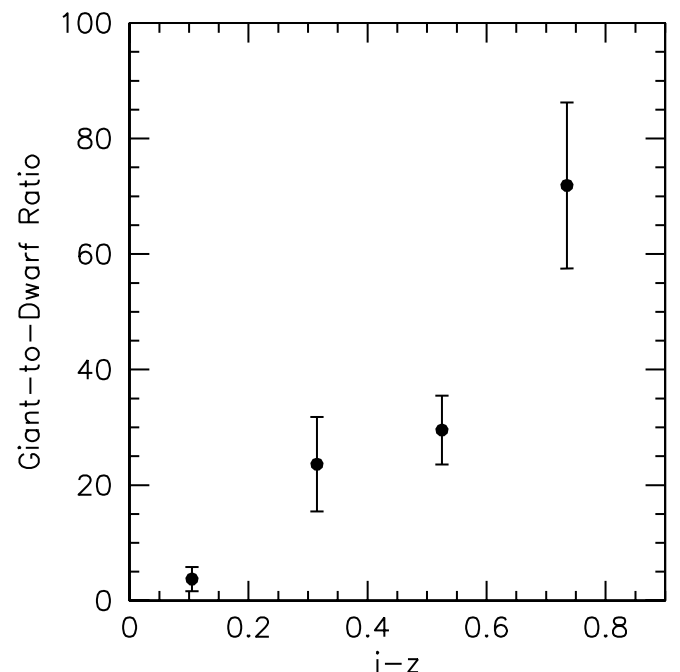


FIG. 11.—Giant-to-dwarf ratio as a function of $i_{775} - z_{850}$ color.

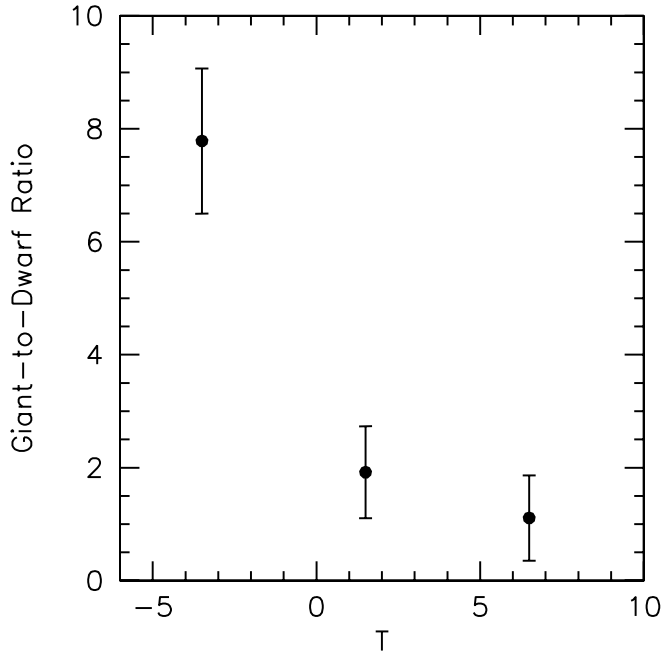


FIG. 12.—Giant-to-dwarf ratio as a function of morphology.

are consistent with the hypothesis that the bright end of the cluster LF is dominated by red or early-type galaxies and the faint end is dominated by blue or late-type galaxies.

In previous sections, we have shown that galaxies in the cluster core (or the densest regions) show different characteristics from galaxies in the cluster outskirts (or the sparsest regions). An important question to ask now is where (in what environment) these changes happen. In Figure 13, we show the GDR as a function of clustocentric distance. The GDR is higher for galaxies in the inner regions of the cluster, consistent with the results shown in Figure 5. In addition, Figure 13 shows that the GDR rises steeply at $R < 0.9$ Mpc, and flattens outside this radius. Similarly in Figure 14, we show the GDR as a function

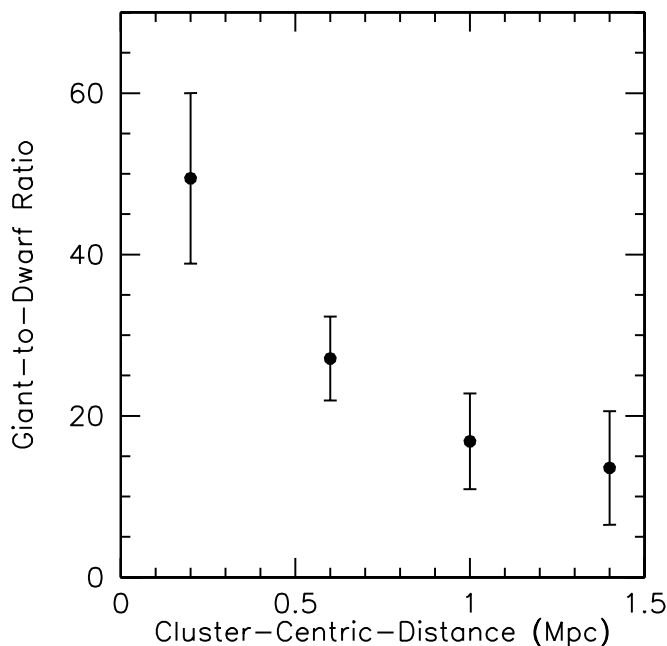


FIG. 13.—Giant-to-dwarf ratio as a function of clustocentric radius.

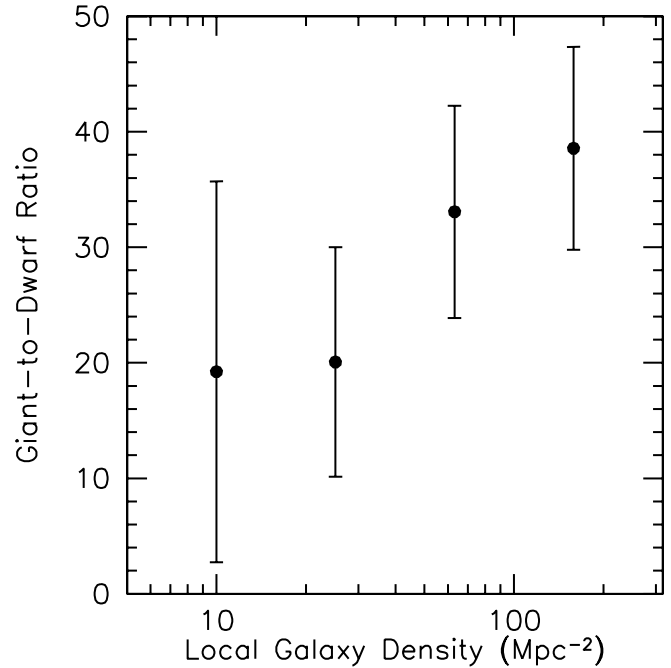


FIG. 14.—Giant-to-dwarf ratio as a function of local galaxy density.

of the local galaxy density (Σ) defined in § 3.3.1. The same trend can be seen here. The GDR rises with increasing local galaxy density. At $\Sigma < 30 \text{ Mpc}^{-2}$, the GDR is consistent with a constant. If MS 1054–0321 were roughly spherical, the deprojected rise in the GDR at small radii would be even steeper. However, MS 1054–0321 is far from spherical, as evidenced by the distributions of the X-ray gas (Donahue et al. 1998; Neumann & Arnaud 2000; Jeltama et al. 2001), the galaxies, and the inferred mass (Luppino & Kaiser 1997; van Dokkum et al. 1999, 2000; Hoekstra et al. 2000; Jee et al. 2005).

5. DISCUSSION

5.1. Comparison with Cluster Luminosity Functions in the Literature

We begin our discussion by comparing the derived LF of MS 1054–0321 with that for cluster galaxies in the local universe. Since the majority of previous work has measured the LFs in the rest-frame B band, we convert our M_i^* to the rest-frame B band for a fair comparison. The conversion is reliable, since the shift between the sampled rest frame at $z = 0.83$ in the i_{775} filter is quite close to the $z = 0$ B -band spectral coverage. As most of the cluster galaxies have passive SEDs (Blakeslee et al. 2003), we use an elliptical galaxy SED template from Benítez et al. (2004) in order to compute the transformation to the B band. The transformed characteristic magnitude for MS 1054–0321 in the rest-frame B band is $M_B^* = -20.35$ ($h = 1$). While not all cluster galaxies have the SED of the elliptical galaxy, the uncertainty introduced by using an elliptical SED for the rest-frame conversion is small because (1) the majority of the galaxies in clusters do exhibit elliptical SEDs and (2) a spiral SED (Sbc in Benítez et al. 2004) yields a transformation that differs by only 0.126 mag, comparable to the statistical error.

Postman et al. (2001) measured $M_B^* = -20.37 \pm 0.17$ for three clusters with a median redshift of 0.859 (all magnitudes we quote in this section are converted to $h = 1$ and are on the Vega magnitude system), in excellent agreement with our MS 1054–0321 results. At low redshift, Colless (1989) measured

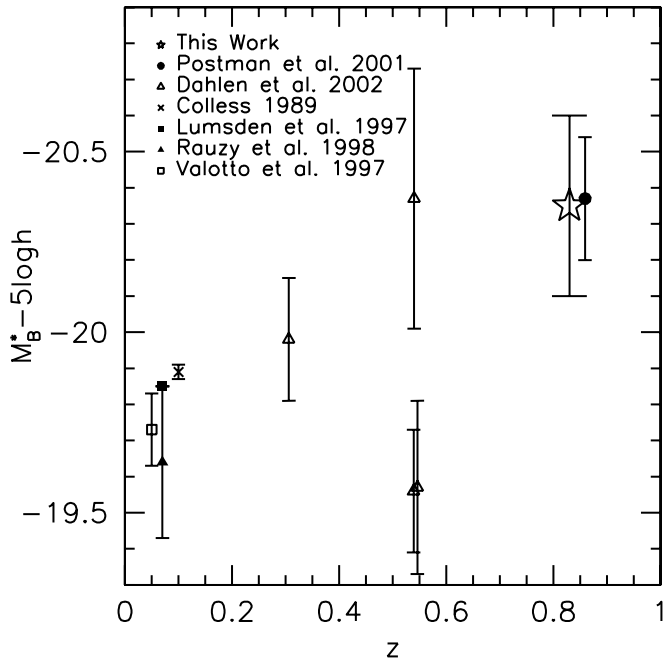


FIG. 15.—Comparison to M_B^* in the literature.

(M_{bj}^*, α) = $(-20.12, -1.24)$ using 14 nearby rich clusters. Lumsden et al. (1997) found (M_{bj}^*, α) = $(-20.16 \pm 0.02, -1.22 \pm 0.04)$ at $z \sim 0.1$. Valotto et al. (1997) found (M_{bj}^*, α) = $(-20.0 \pm 0.1, -1.4 \pm 0.1)$ at $z \sim 0.05$. Rauzy et al. (1998) studied 28 rich clusters with a mean redshift of 0.07, and found (M_{bj}^*, α) = $(-19.91 \pm 0.21, -1.50 \pm 0.11)$. The transformation from B to b_j is $B = b_j + 0.28(B - V)$ (Blair & Gilmore 1982; Cunow 1993). Since a typical $B - V$ color is 0.96 for early-type galaxies (Fukugita et al. 1995), we use $B = b_j + 0.27$. Applying this conversion, we find 0.46–0.71 mag of evolution in M_B^* in clusters between $z = 0$ and 0.83. We summarize these comparisons in Figure 15. The results from Dahlen et al. (2004) appear to have a larger scatter because we plot each cluster as an individual point. However, some caution is required in the interpretation of any LF evolution, because MS 1054–0321 is extremely rich, with $L_X(2-10 \text{ keV}) = 2.2 \times 10^{45} h_{50}^{-1} \text{ ergs s}^{-1}$, and therefore is perhaps not a progenitor of the well-studied low-redshift clusters.

On the other hand, there is significant disagreement with studies on the faint-end slope, α . We find a much flatter faint-end slope. As our study is limited to a single cluster, some of the disagreement may be associated with peculiarities inherent to MS 1054–0321. However, the determination of the faint-end slope depends critically on a good background subtraction and reliable completeness corrections. Hence, some of the difference may also reflect the fact that our analyses are based exclusively on confirmed cluster members. If the deficit of faint red galaxies at high redshift turns out to be real, then some of the difference between our slope and the mean faint end LF slope found at lower redshift may also be related to this underrepresented population component at $z \sim 0.8$. The flat slope in MS 1054–0321 may thus be suggestive of a population of faint red galaxies that is going to be created or accreted into clusters between $0 < z < 0.83$. A similar lack of faint galaxies at high redshift was reported by Kajisawa et al. (2000) and Nakata et al. (2001) in the 3C 324 field, and by De Lucia et al. (2004) in the ESO distant cluster survey at $z = 0.7$ and 0.8. The physics behind the origin of such a galaxy population remains to be ex-

plored. A hint comes from Drinkwater et al. (2003), who find dwarf galaxies without any disk, possibly tidally stripped, in the Fornax Cluster (also see Bekki et al. 2003; Mieske et al. 2004). However, Kodama et al. (2004) reported a lack of faint red galaxies in the high-redshift field regions using the Subaru-*XMM* deep data, and thus the creation of faint galaxies may not be a cluster-specific phenomenon.

5.2. Type-Specific Luminosity Functions

The dependence of the LF on color and morphology in MS 1054–0321 is shown in Figures 8, 9, and 10. In the local universe, Yagi et al. (2002) studied LFs of 10 nearby clusters and find that the LF of galaxies with exponential profiles has a steeper faint-end slope than that for galaxies with $r^{1/4}$ profiles. Similarly, Boyce et al. (2001) studied the LF of A868 ($z = 0.154$) and find that the presence of dwarf irregular galaxies causes the faint-end slope of the cluster LF to steepen. Goto et al. (2002b) used 204 galaxy clusters found in the Sloan Digital Sky Survey (Goto et al. 2002a) to construct composite LFs in $u, g, r, i,$ and z filters. When they divide LFs by morphology and color, the faint-end of the LFs were steeper for late-type (or bluer) galaxies. We also find that the faint-end slope of the LF in MS 1054–0321 is always steeper for blue ($i_{775} - z_{850} < 0.5$) galaxies. These findings are consistent with the hypothesis that the bright end of the cluster LF is dominated by red, early-type galaxies and the faint-end by blue, late-type galaxies.

Considering that field galaxies at around $z \sim 1$ have very different properties from their local counterpart (Kajisawa & Yamada 2001; Cross et al. 2004), it is revealing that these typical characteristics of cluster LFs are already firmly established in a high-redshift galaxy cluster at $z = 0.83$, suggesting that this massive cluster most likely began to form at redshifts considerably greater than unity. A study of a large, statistically complete sample of high-redshift clusters is clearly needed to assess whether the presence of similar LF features is widespread in clusters that existed 6–8 Gyr ago.

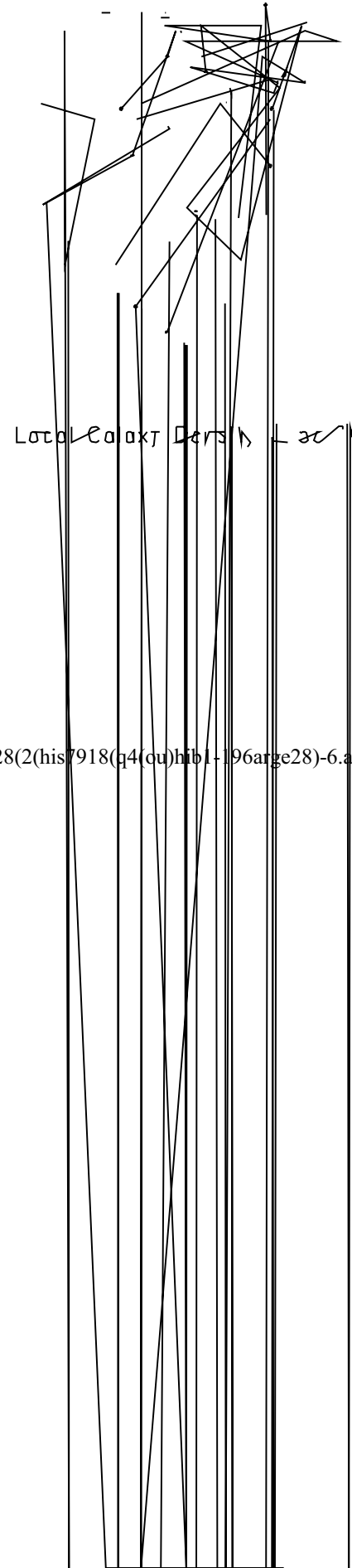
5.3. Comparison with Field Galaxy Luminosity Functions

To gain a better picture of how the cluster environment impacts galaxy-scale stellar systems, we should compare our MS 1054–0321 LF results to those from low-density regions at similar redshifts. Postman et al. (2001) proposed that the evolution of the B -band LFs of field galaxies is consistent with the form $M^*(z) = M(0) - \beta z$, where $1 < \beta < 1.5$. Our cluster M_B^* roughly agrees with the equation within the errors. Cross et al. (2004) have measured LFs of morphologically selected field E/S0 galaxies at $z \sim 0.75$ and find $M_B^* = -20.3 \pm 0.3$ with $\alpha = -0.53 \pm 0.17$. In the Subaru Deep Survey, Kashikawa et al. (2003) derives (M_B^*, α) = $(-20.18_{-0.63}^{+0.26}, -1.07_{-0.07}^{+0.01})$ for field galaxies at $z \sim 1$. Their M_B^* is slightly fainter than the value we obtained for the cluster LF. The α is much steeper than the cluster value we found. These differences are comparable with the differences we find when we compare LF of galaxies in the inner region of the cluster with those in the outskirts of the cluster, i.e., lower density regions have a fainter M^* and steeper faint-end tail. Again, these results are consistent with the hypothesis that cluster regions are dominated by the bright galaxies, and faint galaxies are more numerous in the field regions.

5.4. Luminosity Segregation: Where Does It Happen?

In Figures 13 and 14, we demonstrate that the GDR starts to change at around $R = 0.9 \text{ Mpc}$ or $\Sigma = 40 \text{ Mpc}^{-2}$. In Figure 1, the crosses denote the projected positions on the sky of cluster

members in this transition region with $10 < \Sigma < 40 \text{ Mpc}^{-2}$. As can be seen, this density regime corresponds to the outskirts of the cluster. This environment coincides with that where the relative morphological population fractions and star formation rate (SFR) of galaxies starts to exhibit significant change, at least in $z < 0.1$ surveys. For example, Goto et al. (2003a) studied the morphology-density relation using a large sample from the SDSS to find that galaxy morphology starts to change around the virial radius (Girardi et al. 1996.



7918(44)hib1-196arge28)-6.40(3(ri)56.60(3(21)-4.

1. The faint-end slope of the LFs is steeper in the bluest band (Fig. 4).

2. The LF of galaxies in the inner part of the cluster ($R < 0.9$ Mpc) has a flatter faint-end slope than that in the outer regions ($R \geq 0.9$ Mpc; Fig. 5). The corresponding trend can be seen when the LF is measured as a function of the local galaxy density (Fig. 6).

3. The fraction of early-type galaxies is largest at the bright end of the LF and gradually decreases toward fainter magnitudes (Figs. 9 and 10).

4. The trends seen in (1), (2), and (3) are generally in agreement with observations of local galaxy clusters showing that the cluster core regions are dominated by bright early-type galaxies. Hence, a LF similar to what is seen at low redshift is well established in MS 1054–0321, suggesting that, on average, the galaxies in this massive cluster began their formation at redshifts considerably greater than unity.

5. When the LF is partitioned by $i_{775} - z_{850}$ color, we find a marginally significant ($\sim 2\sigma$) deficit of faint red galaxies ($i_{775} - z_{850} \geq 0.5$, $M_i > -19$). The deficit is inferred as well when we analyze the LF as a function of morphology—a possible lack of early-type galaxies in the faintest bin (Fig. 9). If real, these trends may suggest that faint, red, early-type galaxies have not been yet

created in MS 1054–0321. A deficit of such galaxies has not been seen in low- z clusters.

6. The giant-to-dwarf ratio exhibits a strong radial dependence beginning at around the virial radius, or a strong density dependence when the density increases above $\Sigma \sim 30 \text{ Mpc}^{-2}$. The ratio is higher in the inner parts (or higher density regions) of the cluster (Figs. 13 and 14). This environment roughly corresponds to the same location at which galaxy color and the morphology start to vary significantly with position and density (Figs. 16 and 17). A physical process effective at this environment, such as galaxy merging, may be responsible for the cluster galaxy evolution in these transition regions.

We thank the anonymous referee for providing constructive and insightful comments that have greatly improved the clarity of this paper. We also thank Pieter G. van Dokkum for very useful comments. The ACS was developed under NASA contract NAS 5-32865, and this research is supported by NASA grant NAG5-7697. Some of the results in this paper were based on computations performed on equipment generously provided through a grant from Sun Microsystems, Inc.

REFERENCES

- Abadi, M. G., Moore, B., & Bower, R. G. 1999, *MNRAS*, 308, 947
 Andreon, S. 1998, *ApJ*, 501, 533
 ———. 2001, *ApJ*, 547, 623
 Andreon, S., & Etori, S. 1999, *ApJ*, 516, 647
 Andreon, S., Lobo, C., & Iovino, A. 2004, *MNRAS*, 349, 889
 Bekki, K. 1998, *ApJ*, 502, L133
 Bekki, K., Couch, W. J., Drinkwater, M. J., & Shioya, Y. 2003, *MNRAS*, 344, 399
 Bekki, K., Couch, W. J., & Shioya, Y. 2002, *ApJ*, 577, 651
 Benítez, N., Broadhurst, T., Rosati, P., Courbin, F., Squires, G., Lidman, C., & Magain, P. 1999, *ApJ*, 527, 31
 Benítez, N., et al. 2004, *ApJS*, 150, 1
 Bennett, C. L., et al. 2003, *ApJS*, 148, 1
 Bernstein, G. M., Nichol, R. C., Tyson, J. A., Ulmer, M. P., & Wittman, D. 1995, *AJ*, 110, 1507
 Binggeli, B., & Jerjen, H. 1998, *A&A*, 333, 17
 Binggeli, B., Sandage, A., & Tammann, G. A. 1988, *ARA&A*, 26, 509
 Blair, M., & Gilmore, G. 1982, *PASP*, 94, 742
 Blakeslee, J. P., et al. 2003, *ApJ*, 589, 693
 Boyce, P. J., Phillipps, S., Jones, J. B., Driver, S. P., Smith, R. M., & Couch, W. J. 2001, *MNRAS*, 328, 277
 Butcher, H., & Oemler, A. 1978, *ApJ*, 219, 18
 ———. 1984, *ApJ*, 285, 426
 Byrd, G., & Valtonen, M. 1990, *ApJ*, 350, 89
 Colless, M. 1989, *MNRAS*, 237, 799
 Couch, W. J., Barger, A. J., Smail, I., Ellis, R. S., & Sharples, R. M. 1998, *ApJ*, 497, 188
 Couch, W. J., Ellis, R. S., Sharples, R. M., & Smail, I. 1994, *ApJ*, 430, 121
 Cowie, L. L., & Songaila, A. 1977, *Nature*, 266, 501
 Cross, N., et al. 2004, *AJ*, 128, 1990
 Cuesta-Bolao, M. J., & Serna, A. 2003, *A&A*, 405, 917
 Cunow, B. 1993, *A&AS*, 97, 541
 Dahlén, T., Fransson, C., Östlin, G., & Näslund, M. 2004, *MNRAS*, 350, 253
 De Lucia, G., et al. 2004, *ApJ*, 610, L77
 de Propris, R., Eisenhardt, P. R., Stanford, S. A., & Dickinson, M. 1998, *ApJ*, 503, L45
 de Propris, R., Stanford, S. A., Eisenhardt, P. R., Dickinson, M., & Elston, R. 1999, *AJ*, 118, 719
 De Propris, R., et al. 2003, *MNRAS*, 342, 725
 Donahue, M., Voit, G. M., Gioia, I., Lupino, G., Hughes, J. P., & Stocke, J. T. 1998, *ApJ*, 502, 550
 Dressler, A., & Gunn, J. E. 1992, *ApJS*, 78, 1
 Dressler, A., Smail, I., Poggianti, B. M., Butcher, H., Couch, W. J., Ellis, R. S., & Oemler, A. J. 1999, *ApJS*, 122, 51
 Dressler, A., et al. 1997, *ApJ*, 490, 577
 Drinkwater, M. J., Gregg, M. D., Hilker, M., Bekki, K., Couch, W. J., Ferguson, H. C., Jones, J. B., & Phillipps, S. 2003, *Nature*, 423, 519
 Driver, S. P., Couch, W. J., & Phillipps, S. 1998, *MNRAS*, 301, 369
 Driver, S. P., Phillipps, S., Davies, J. I., Morgan, I., & Disney, M. J. 1994, *MNRAS*, 268, 393
 Ellingson, E., Lin, H., Yee, H. K. C., & Carlberg, R. G. 2001, *ApJ*, 547, 609
 Fabricant, D., Franx, M., & van Dokkum, P. 2000, *ApJ*, 539, 577
 Farouki, R., & Shapiro, S. L. 1980, *ApJ*, 241, 928
 Fasano, G., Poggianti, B. M., Couch, W. J., Bettoni, D., Kjaergaard, P., & Moles, M. 2000, *ApJ*, 542, 673
 Ferguson, H. C., & Sandage, A. 1991, *AJ*, 101, 765
 Finoguenov, A., Briel, U. G., & Henry, J. P. 2003, *A&A*, 410, 777
 Fujita, Y. 1998, *ApJ*, 509, 587
 ———. 2004, *PASJ*, 56, 29
 Fujita, Y., & Goto, T. 2004, *PASJ*, 56, 621
 Fujita, Y., & Nagashima, M. 1999, *ApJ*, 516, 619
 Fukugita, M., Shimasaku, K., & Ichikawa, T. 1995, *PASP*, 107, 945
 Garilli, B., Maccagni, D., & Andreon, S. 1999, *A&A*, 342, 408
 Gioia, I. M., Braitto, V., Branchesi, M., Della Ceca, R., Maccacaro, T., & Tran, K.-V. 2004, *A&A*, 419, 517
 Gioia, I. M., Maccacaro, T., Schild, R. E., Wolter, A., Stocke, J. T., Morris, S. L., & Henry, J. P. 1990, *ApJS*, 72, 567
 Girardi, M., Giuricin, G., Mardirossian, F., Mezzetti, M., & Boschin, W. 1998, *ApJ*, 505, 74
 Gnedin, O. Y. 2003a, *ApJ*, 582, 141
 ———. 2003b, *ApJ*, 589, 752
 Goto, T., Yagi, M., Tanaka, M., & Okamura, S. 2004a, *MNRAS*, 348, 515
 Goto, T., Yamauchi, C., Fujita, Y., Okamura, S., Sekiguchi, M., Smail, I., Bernardi, M., & Gomez, P. L. 2003a, *MNRAS*, 346, 601
 Goto, T., et al. 2002a, *AJ*, 123, 1807
 ———. 2002b, *PASJ*, 54, 515
 ———. 2003b, *PASJ*, 55, 739
 ———. 2003c, *PASJ*, 55, 771
 ———. 2004b, *ApJ*, submitted
 Gunn, J. E., & Gott, J. R. I. 1972, *ApJ*, 176, 1
 Haines, C. P., Clowes, R. G., Campusano, L. E., & Adamson, A. J. 2001, *MNRAS*, 323, 688
 Hoekstra, H., Franx, M., & Kuijken, K. 2000, *ApJ*, 532, 88
 Icke, V. 1985, *A&A*, 144, 115
 Jee, J., et al. 2005, *ApJ*, submitted
 Jeltrema, T. E., Canizares, C. R., Bautz, M. W., Malm, M. R., Donahue, M., & Garmire, G. P. 2001, *ApJ*, 562, 124
 Jones, L., Smail, I., & Couch, W. J. 2000, *ApJ*, 528, 118
 Kajisawa, M., & Yamada, T. 2001, *PASJ*, 53, 833
 Kajisawa, M., et al. 2000, *PASJ*, 52, 61

- Kashikawa, N., et al. 2003, *AJ*, 125, 53
- Kent, S. M. 1981, *ApJ*, 245, 805
- Kodama, T., & Bower, R. G. 2001, *MNRAS*, 321, 18
- Kodama, T., Smail, I., Nakata, F., Okamura, S., & Bower, R. G. 2001, *ApJ*, 562, L9
- Kodama, T., et al. 2004, *MNRAS*, 350, 1005
- Koo, D. C., & Kron, R. G. 1992, *ARA&A*, 30, 613
- Larson, R. B., Tinsley, B. M., & Caldwell, C. N. 1980, *ApJ*, 237, 692
- Lavery, R. J., & Henry, J. P. 1988, *ApJ*, 330, 596
- Lidman, C., Rosati, P., Demarco, R., Nonino, M., Mainieri, V., Stanford, S. A., & Toft, S. 2004, *A&A*, 416, 829
- Lin, Y., et al. 2004, *ApJ*, 610, 745
- Lugger, P. M. 1986, *ApJ*, 303, 535
- Lumsden, S. L., Collins, C. A., Nichol, R. C., Eke, V. R., & Guzzo, L. 1997, *MNRAS*, 290, 119
- Luppino, G. A., & Kaiser, N. 1997, *ApJ*, 475, 20
- Makino, J., & Hut, P. 1997, *ApJ*, 481, 83
- Mamon, G. A. 1992, *ApJ*, 401, L3
- Mamon, G. A., Sanchis, T., Salvador-Solé, E., & Solanes, J. M. 2004, *A&A*, 414, 445
- Margoniner, V. E., & de Carvalho, R. R. 2000, *AJ*, 119, 1562
- Margoniner, V. E., de Carvalho, R. R., Gal, R. R., & Djorgovski, S. G. 2001, *ApJ*, 548, L143
- Martínez, H. J., Zandivarez, A., Merchán, M. E., & Domínguez, M. J. L. 2002, *MNRAS*, 337, 1441
- Mercurio, A., Massarotti, M., Merluzzi, P., Girardi, M., La Barbera, F., & Busarello, G. 2003, *A&A*, 408, 57
- Mieske, S., et al. 2004, *AJ*, 128, 1529
- Molinari, E., Chincarini, G., Moretti, A., & de Grandi, S. 1998, *A&A*, 338, 874
- Moore, B., Diemand, J., & Stadel, J. 2004, in *Proc. IAU Colloq. 195, Outskirts of Galaxy Clusters: Intense Life in the Suburbs*, ed. A. Diaferio (Cambridge: Cambridge Univ. Press), in press (astro-ph/0406615)
- Moore, B., Katz, N., Lake, G., Dressler, A., & Oemler, A. 1996, *Nature*, 379, 613
- Moore, B., Lake, G., Quinn, T., & Stadel, J. 1999, *MNRAS*, 304, 465
- Nakata, F., et al. 2001, *PASJ*, 53, 1139
- Neumann, D. M., & Arnaud, M. 2000, *ApJ*, 542, 35
- Oke, J. B., et al. 1995, *PASP*, 107, 375
- Ostriker, J. P. 1993, *ARA&A*, 31, 689
- Paolillo, M., Andreon, S., Longo, G., Puddu, E., Gal, R. R., Scaramella, R., Djorgovski, S. G., & de Carvalho, R. 2001, *A&A*, 367, 59
- Parolin, I., Molinari, E., & Chincarini, G. 2003, *A&A*, 407, 823
- Phillipps, S., Driver, S. P., Couch, W. J., & Smith, R. M. 1998, *ApJ*, 498, L119
- Poggianti, B. M., Smail, I., Dressler, A., Couch, W. J., Barger, A. J., Butcher, H., Ellis, R. S., & Oemler, A. J. 1999, *ApJ*, 518, 576
- Postman, M., & Geller, M. J. 1984, *ApJ*, 281, 95
- Postman, M., Lubin, L. M., & Oke, J. B. 1998, *AJ*, 116, 560
- . 2001, *AJ*, 122, 1125
- Postman, M., et al. 2005, *ApJ*, in press
- Quilis, V., Moore, B., & Bower, R. 2000, *Science*, 288, 1617
- Rakos, K. D., & Schombert, J. M. 1995, *ApJ*, 439, 47
- Rauzy, S., Adami, C., & Mazure, A. 1998, *A&A*, 337, 31
- Rosati, P., Stanford, S. A., Eisenhardt, P. R., Elston, R., Spinrad, H., Stern, D., & Dey, A. 1999, *AJ*, 118, 76
- Schechter, P. 1976, *ApJ*, 203, 297
- Schlegel, D. J., Finkbeiner, D. P., & Davis, M. 1998, *ApJ*, 500, 525
- Secker, J., & Harris, W. E. 1996, *ApJ*, 469, 623
- Stanford, S. A., Elston, R., Eisenhardt, P. R., Spinrad, H., Stern, D., & Dey, A. 1997, *AJ*, 114, 2232
- Tanaka, M., Goto, T., Shimasaku, M., & Okamura, S. 2004, *AJ*, 128, 2677
- Tanaka, I., Yamada, T., Aragón-Salamanca, A., Kodama, T., Miyaji, T., Ohta, K., & Arimoto, N. 2000, *ApJ*, 528, 123
- Toft, S., Mainieri, V., Rosati, P., Lidman, C., Demarco, R., Nonino, M., & Stanford, S. A. 2004, *A&A*, 422, 29
- Tran, K. H., Kelson, D. D., van Dokkum, P., Franx, M., Illingworth, G. D., & Magee, D. 1999, *ApJ*, 522, 39
- Trentham, N. 1998, *MNRAS*, 294, 193
- Treu, T., Ellis, R. S., Kneib, J., Dressler, A., Smail, I., Czoske, O., Oemler, A., & Natarajan, P. 2003, *ApJ*, 591, 53
- Valluri, M. 1993, *ApJ*, 408, 57
- Valotto, C. A., Moore, B., & Lambas, D. G. 2001, *ApJ*, 546, 157
- Valotto, C. A., Nicotra, M. A., Muriel, H., & Lambas, D. G. 1997, *ApJ*, 479, 90
- van Dokkum, P. G., Franx, M., Fabricant, D., Illingworth, G. D., & Kelson, D. D. 2000, *ApJ*, 541, 95
- van Dokkum, P. G., Franx, M., Fabricant, D., Kelson, D. D., & Illingworth, G. D. 1999, *ApJ*, 520, L95
- van Dokkum, P. G., Franx, M., Kelson, D. D., & Illingworth, G. D. 1998, *ApJ*, 504, L17
- van Dokkum, P. G., Stanford, S. A., Holden, B. P., Eisenhardt, P. R., Dickinson, M., & Elston, R. 2001, *ApJ*, 552, L101
- Yagi, M., Kashikawa, N., Sekiguchi, M., Doi, M., Yasuda, N., Shimasaku, K., & Okamura, S. 2002, *AJ*, 123, 87
- Yamauchi, C., & Goto, T. 2004, *MNRAS*, 352, 815